6-1980

Probabilistic Models for Defect Initiated Fracture in Ceramics

A. G. Evans
University of California - Berkeley

M. E. Meyer
Rockwell International

K. W. Fertig
Rockwell International

B. I. Davis
Rockwell International

H. R. Baumgartner
Norton Co.

Probabilistic Models for Defect Initiated Fracture in Ceramics

Abstract
Fracture tests on hot-pressed silicon nitride containing voids and several types of inclusions have been conducted. Fracture models pertinent to each defect type have been proposed and correlated with the data. The specificity of the fracture models is emphasized, and the various trends with defect size that result from the models are described. The resultant fracture probability relations are one of the key inputs to accept/reject decisions for nondestructive failure prediction.

Keywords
Nondestructive Evaluation

Disciplines
Materials Science and Engineering

PROBABILISTIC MODELS FOR DEFECT INITIATED FRACTURE IN CERAMICS

A. G. Evans
University of California
Berkeley, California 94720

M. E. Meyer, K. W. Fertig and B. I. Davis
Rockwell International Science Center
Thousand Oaks, California 91360

H. R. Baumgartner
Norton Co.
Worcester, Massachusetts 01606

ABSTRACT

Fracture tests on hot-pressed silicon nitride containing voids and several types of inclusions have been conducted. Fracture models pertinent to each defect type have been proposed and correlated with the data. The specificity of the fracture models is emphasized, and the various trends with defect size that result from the models are described. The resultant fracture probability relations are one of the key inputs to accept/reject decisions for nondestructive failure prediction.

INTRODUCTION

Inclusions and voids are important sources of failure in structural ceramics. It is crucial for the structural utilization of these materials that the probability of fracture from typical defects be sufficiently characterized that effective nondestructive failure prediction schemes can be devised. In this study, samples of silicon nitride containing typical defects are subjected to controlled fracture tests to determine both the fracture mechanism and the specific fracture stress at the defect. Fracture models pertinent to each defect type are then developed, and the fracture probabilities (derived from the test data) are related to the parameters of the models. The resultant probability functions constitute one of the three functions required to isolate the accept/reject criterion pertinent to nondestructive failure prediction.[1]

Preliminary studies of fracture from defects in ceramics[2-5] have indicated that the fracture process is likely to consist of the activation of small defects (voids, disbonds, grain boundary cracks), occurring within or near the defect, by the ambient local stress field (due to both the thermal expansion mismatch and the applied stress). Usually, the influence of the defect on strength is expected to be less severe than that of a crack of equivalent dimensions.[2-5] The important exception is an inclusion with both a thermal expansion coefficient and a bulk modulus lower than the host material (then, large radial cracks can develop that substantially reduce the strength). However, the incidence of such inclusions in structural ceramics (such as silicon nitride) is expected to be minimal, because these materials have a low intrinsic thermal expansion coefficient.

The inherent flaws that initiate inclusion fracture are likely to be statistically distributed in size and space. Therefore, the fracture stress should not be expected to relate uniquely to the defect dimensions, but rather, to exhibit a distribution of values for each defect size.[4,5] The determination of the pertinent fracture distribution functions is the primary objective of the present study.

EXPERIMENTAL

Technique - Samples containing the defect types that predominate in hot-pressed silicon nitride (Table 1) were specially fabricated* in two sets. One set consisted of 2.5 cm diameter discs with the defects approximately located at the disc center. The other set consisted of oversized bars containing inclusions, later to be machined to final dimensions suitable for flexure testing. The samples were inspected using advanced ultrasonic techniques to determine the precise location of the dominant defect. The samples were then machined until the defect was located ~200 μm from one surface of the sample. This operation was conducted to ensure that the defect would be subjected to an appreciable tensile stress during subsequent flexure testing. Therefore, each sample was annealed, in air at 1000°C for ~20 hr., to minimize the influence of surface cracks introduced during the grinding process. Finally, the samples were subjected to flexural, constant displacement-rate fracture tests conducted at room temperature. Those samples with defects located at the disc center were tested in biaxial flexture.[6] Samples with defects displaced from the disc center were put into beams (20 cm x 5 mm x 5 mm), such that the defect was located at the beam center, and then tested in three-point flexure. Acoustic emission was monitored on each sample throughout the test. The bar samples were also machined into beams (38 mm x 6 mm x 3 mm), and tested in four-point flexure such that the inclusions were between the inner span supports. After strength testing, fracture faces were examined by microscopy and microprobe to verify the location and nature of fracture origins.

Results - The results of the fracture were used to calculate the stress at the center plane of the defect, at the condition of fracture instability. These defect fracture stresses are summarized in Table I. The acoustic emission record did not generally indicate well-defined pre-fracture emission, except for the silicon inclusions, which exhibited consistent emission at about one-tenth of the the final fracture load.

*The fabrication was conducted by the Norton Co., Worcester, Massachusetts.

The dimensions of the fracture initiating defects on the fracture plane were measured on each sample, as summarized in Table I. Also, for samples in which defect removal could be effected, the defect volumes were measured. The detailed volume measurement technique is described in Appendix II. The results are summarized in Table I. As a general comparison, the present results are combined with other results* to plot trends in the average strength with defect-size (Fig. 1). The strong role of defect type on strength is immediately apparent.

TABLE 1

Defect Type	Stress at (MPa) Defect	Defect size z(μ)	x(μm)	V(m^3)
Silicon	400	50	265	-
	362	100	475	-
	375	75	425	-
	264	125	625	-
	243	250	875	-
	283	125	875	-
	272	250	675	-
	410	75	200	-
	432	75	275	-
	284	175	425	-
	357	100	100	-
	424	75	250	-
	434	50	100	-
	265	175	750	-
	252	125	625	-
Iron	398			2.5×10^{-12}
	323			1.6×10^{-11}
	383			9.1×10^{12}
	334			2.2×10^{-11}
	355			3.1×10^{-11}
	210			3.9×10^{-10}
	217			3.1×10^{-10}
	404			6.2×10^{-13}
	258			7.0×10^{-11}
	296			6.1×10^{-11}
	333			3.3×10^{-11}
	283			6.5×10^{-11}
	173			2.9×10^{-10}
	281			1.1×10^{-10}
	206			3.2×10^{-10}
	190			3.0×10^{-10}
	268			1.8×10^{-10}
Tungsten Carbide	550	75	175	
	590	125	150	
	560	75	300	
	610	400	675	
	600	100	300	
	480	400	400	
Void	365	250	250	
	317	250	250	
	316	250	250	
	314	250	250	
	302	250	250	
	293	250	250	
	265	250	250	
	365	250	250	
	317	250	250	

*Results obtained from, H.R. Baumgartner, R.H. Brockelman and P.M. Hansen, AMMRC Report TR 78-11 (June 1978) and from; J.J. Petrovic and M.G. Merdiratta, Jnl. Amer. Ceram. Soc., 59 (1976) 163.

TABLE 1 (Cont'd)

Defect Type	Stress at (MPa) Defect	Defect Size z(μm)	x(μm)	V(m^3)
Void	316	250	250	
	314	250	250	
	302	250	250	
	293	250	250	
	265	250	250	
	265	250	250	
	248	250	250	
	248	250	250	
	247	250	250	
	246	250	250	
	226	250	250	
	206	250	250	
	191	250	250	
	181	250	250	
	165	250	250	
	234	500	500	
	224	500	500	
	211	500	500	
	210	500	500	
	194	500	500	
	197	500	500	
	185	500	500	
	178	500	500	
	177	500	500	
	176	500	500	
	153	500	500	
	145	500	500	
	140	500	500	
	126	500	500	
	109	500	500	
	100	500	500	
	434	44	48*	

*Result obtained from: F. I. Barratta, G. W. Driscoll and R. N. Katz, Ceramics For High Performance. Applications (Ed., J. J. Burke, A. G. Gorum and R.N. Katz), Brooke Hill, MA (1974) p. 445.

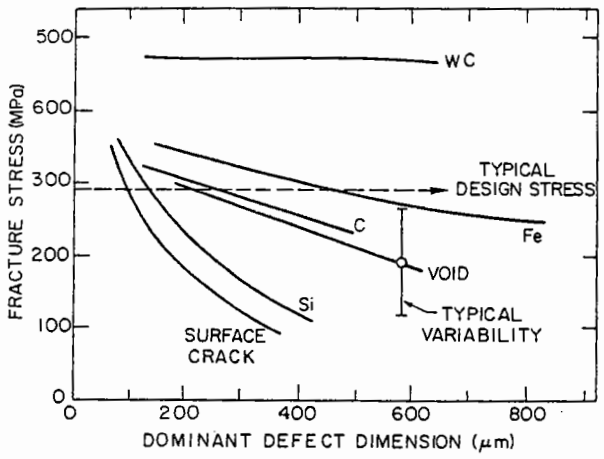

Fig. 1 A plot of trends in the average fracture strength with defect size for several different defect types in silicon nitride.

FRACTURE MODELS

General Considerations - It is instructive to provide a perspective of defect fracture by examining the stress fields associated with defects, and thereby, to identify the possible modes of fracture. (The fracture modes that occur for inclusions with a lower expansion coefficient than the matrix are excluded from consideration, as noted in the Introduction.)

The thermal expansion mismatch introduces hydrostatic tension within inclusions. The magnitude of this stress, σ_α, is given by[7,8]

$$\sigma_\alpha = \frac{4G_m \Delta\alpha \, \Delta T}{1 + [2(1-2\nu_i)/(1+\nu_i)](G_m/G_i)} \equiv \beta \qquad (1)$$

where $\Delta\alpha$ is the differential thermal expansion coefficient, ΔT is the temperature differential, G is the shear modulus, ν is Poisson's ratio and the subscripts m and i refer to the matrix and inclusion, respectively. The equivalent stresses within the matrix are, for a spherical inclusion with radius R,

$$\sigma_{rr} = \beta^* (R/r)^3 \qquad (2)$$

$$\sigma_{\theta\theta} = -\beta^* (R/r)^3/2$$

The application of a stress σ_∞ generates additional stresses within the inclusion. For a spherical defect and an applied pressure p_∞, the stress in the defect is given by[8]:

$$\frac{p_i}{p_\infty} = 1 + \frac{2[(\kappa_i/\kappa_m)-1](1-2\nu)}{3(1-\nu)} \left[\frac{4G_m+3\kappa_m}{4G_m+3\kappa_i}\right] \qquad (3)$$

where κ is the bulk modulus.

The significance of these local stresses depends on the distribution of flaws within the defect, matrix and interface; as well as the intrinsic toughness (of inclusion and matrix). When the toughness of an inclusion is appreciably larger than that of the matrix (as might pertain for WC inclusions in Si_3N_4), fracture will tend to initiate within the matrix, from flaws located either at the interface or within the matrix itself (Fig. 2). In this case, the location of fracture and the fracture probability depend primarily on the ratio of the inclusion and matrix elastic constants. Specifically, for inclusions with a smaller modulus than the matrix, the maximum local tensile stress occurs at the equatorial plane,[8] and fracture will initiate from flaws located in this vicinity, as indicated in Fig. 2(a). For inclusions with a higher modulus than the matrix, the maximum local tension (in the appropriate orientation for continued extension into the matrix, i.e., normal to σ_∞) occurs at the poles of the inclusion[8] (Fig. 2(b)). However, both the maximum tension and the extent of the

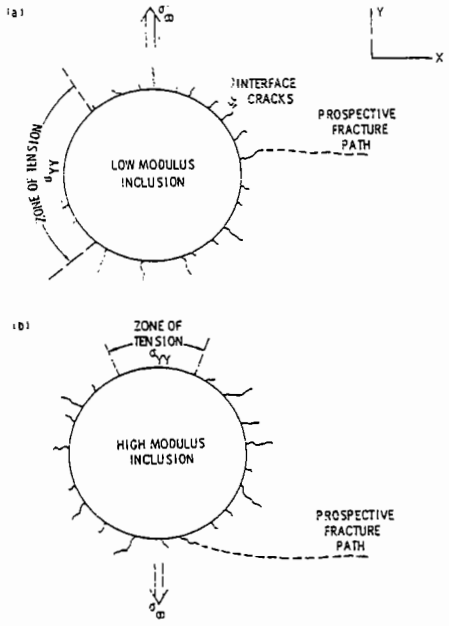

Fig. 2 Schematics indicating fracture initiation within the matrix from interface interface microcracks for (a) low modulus inclusions and (b) high modulus inclusions.

tensile zone are appreciably smaller (for the same modulus mismatch) than the equivalent quantities for the low modulus inclusions. The probability of fracture from the latter is thus anticipated to be relatively low.

A more typical condition involves inclusions with a lower fracture toughness than the matrix. Then, inclusion fracture may occur. When the inclusion has a relatively high modulus (although not necessarily higher than that of the matrix), so that appreciable stresses develop within the inclusion, the fracture of the inclusion can be subcritical, i.e., an additional stress is required to initiate structural failure. Alternatively, if the inclusion has a low modulus (e.g., a porous inclusion, see Appendix I), the stress within the inclusion is low and inclusion fracture might then coincide with structural failure.

This multiplicity of fracture modes requires that each inclusion type be evaluated on an individual basis. The subsequent analysis comprises separate sections for each of the defect types listed in Table I.

Specific Fracture Models

Voids - Previous studies[4,5] have suggested that fracture from voids occurs by the activation of microcracks located on (or near) the surface of the voids (see Fig. 2a). A combined fracture mechanics, statistical analysis of this problem yielded the following relation for the fracture probability, Φ, at the stress S[5];

$$\Phi = 1-\exp\left\{[-8R^2(S/S_o)^m \exp(0.52m-1.4)D^m(\alpha)]\right\} \quad (4)$$

where S_o is the scale parameter, m the shape parameter, R is the void radius; α is given by;

$$\alpha = (1/R)\ (K_c/S)^2 \quad (5)$$

where K_c is the effective microcrack extension resistance and $D(\alpha)$ has the approximate form,

$$D(\alpha) \approx 0.3 + 0.7[1+(\alpha/2)^2]^{-1} \quad (6)$$

The conformance of the test data to the predictions of this model is assessed by separately estimating the dependence of the data on the radius R of the void and on the stress level S. This is achieved through a generalization of Eq. (4);

$$\Phi(x|r) = P[S<x|R=r]$$

$$= 1-\exp[-g(r,\beta) \int_0^x \lambda_o(u)du] \quad (7)$$

where $g(r,\beta)$ is of known functional form (except for the parameter β) and independent of the value of S, while $\lambda_o(u)$ is independent of the value of R. For the present problem Eq. (7) can be written as

$$\Phi(x|r) = 1-\exp[-r^\beta \int_0^x \lambda_o(u)du] \quad (8)$$

We commence the analysis by supposing that the term $D(\alpha)$ is relatively invariant within the range of the test data. Then, the hypotheses of the fracture model are:

$$\beta = 2$$

$$\lambda_o(u) = \frac{m}{S_o}\left(\frac{u}{S_o}\right)^{m-1} \quad (9)$$

The influence of the radius is examined first, by comparing the formal statement of the null hypothesis, H_o: $\beta=2$, with the alternative, H_1: $\beta\neq 2$. A procedure devised by Cox[9], which is independent of the functional form of $\lambda_o(u)$, is used for this purpose. Let the observed failure stresses for samples k_1, k_2.....k_n be, $o<u_1<u_2$ .....u_n, where no ties are allowed. Let $R(u_j)$ be the set of all items surviving until just before the j'th failure. Then, the partial likelihood function L_p is;

$$L_p = \prod_{j=1}^{N} \frac{r_{k_j}}{\sum_{i\in R(u_j)} r_{k_i}^\beta} \quad (10)$$

Under the null hypothesis H_o that $\beta=2$, the statistic $(\partial \ell n\ L_p/\partial\beta)^2(-\partial^2 \ell n\ L_p/\partial\beta^2)^{-1}$ is asympototically distributed as a chi-square random variable with one degree of freedom. Hence, for large samples, it can be used as a test statistic for the null hypothesis, H_o. For the test data pertinent to void initiated fracture summarized in Table I, application of the above result yields a test statistic of 1.80. This value has an asymptotic significance level of 0.18 and, therefore, the null hypothesis that $\beta = 2$ appears to be supported by the data. The maximum likelihood estimate of β was also obtained from

$$\frac{\partial \ell n\ L_p}{\partial\beta} = 0\ , \quad (11)$$

yielding a value, $\hat{\beta} = 3.03$.

The consistency of the test data with the simplified model, $\beta = 2$, does not exclude the possibility that for small (or large) voids an additional dependence on R may emerge from $D(\alpha)$. Additional data will be required to examine this possibility.

The analysis can now proceed, by testing the hypothesis that the parameters m and S_o do not depend on the radius r_i, through the restated model

$$-\ell n[1-\Phi(x_i|r_i)] = r_i^2\left[\frac{x}{S_o(r_i)}\right]^{M(r_i)} \quad (12)$$

where r_i is fixed for each data sample. Since there are two samples (r_i = 125μm and r_i = 250μm), the intent is to test the null hypothesis

$$H_o : \begin{cases} m(125) = m(250) = m \\ S_o(125 = S_o(250) = S_o \end{cases}$$

versus the alternate hypothesis

$$H_1 : \begin{cases} m(125) \neq m(250) \quad \text{or} \\ S_o(125) \neq S_o(250) \end{cases}$$

To test the relative merits of H_o versus H_1, the likelihood ratio statistic ℓ was obtained. Noting that $-2\ell n\ell$ is distributed as a chi-square random variable (with two degrees of freedom), the analysis yielded the result, $-2\ell n\ell = 2.709$, which is not significant at the 0.25 level. Hence, on the basis of this test, the data support the null hypothesis H_o, that m and S_o are independent of

the void radius. A Weibull goodness of fit test also strongly supports the hypothesis. Maximum likelihood estimates obtained for the scale and shape parameters are;

$$\hat{S}_o = 106.3 \quad \text{MPa}$$

$$\hat{m} = 4.57$$

As a final assessment of the model, the fracture probability associated with the test result obtained for the 44μm diameter void is, derived from the above estimates of $\hat{\beta}$, $\hat{m}$ and $\hat{S}_o$. This analysis provides a fracture probability of 0.25, which is quite reasonable.

The application of the test results to the prediction of failure or survival ideally requires that a maximum likelihood estimate be derived. This estimate, described in Appendix III, is given by;

$$\hat{P}\,[S > x | R = r] \tag{13}$$

$$= \prod_{\{k \leq x\}} \left[1 - \frac{r_k^2}{\sum_{k \leq \ell \leq N} r_\ell^2} \right]^{(r/r_k)^2}$$

Inclusions

Silicon Inclusions - The silicon inclusions observed on the fracture surface are characterized by a lack of porosity, signifying (see Appendix I) that there is little thermal expansion mismatch at temperatures above ~1000°C (the temperature at which stress relaxation by mass transport becomes slow). This can be rationalized by noting that the large thermal contraction of the silicon between 1000 and 1800°C is counteracted by the unusual volume expansion that occurs during solidification. Between 1000°C and 30°C the total contraction of the silicon is very similar to that of silicon nitride: indicating that the thermal mismatch stresses in the silicon inclusions should be small.

Dense silicon has elastic properties appreciably lower than those of silicon nitride (Young's moduli of 110 and 320 GPa, respectively). These relative properties lead to a stress in the inclusion $\sigma_i \approx 0.64\ \sigma_\infty$ (see Eq. 3). However, silicon has a very low fracture toughness (0.6 MPa$\sqrt{m}$) compared with the silicon nitride matrix (5 MPa$\sqrt{m}$); so that, despite the low stress level in the inclusion, the inclusion is liable to subcritical fracture. This interpretation is consistent with the acoustic emission measurements (Section 2).

The subcritical fracture of the silicon inclusion introduces a crack with dimensions dictated by the boundaries of the inclusion. The cracked inclusion produces a complex stress intensification of the type[11]:

$$K_I = Z(a/c)F(G_i/G_m)\sigma_\infty a^b \tag{14}$$

where Z is a function of the crack shape, F is a function of the relative elastic moduli and b is a constant ranging from 0.3 to 0.7. The present fracture model is developed on the premise that the modulus mismatch is small and that the cracked inclusion can be treated as a crack in a homogeneous body. (This simplification is necessary at the present level of comprehension of the crack/inclusion problem, and will evidently introduce an error into the fracture characterization.) Then, introducing the macro-toughness of silicon nitride and the inclusion dimensions (on the fracture surface), the predicted fracture stress σ_p becomes

$$\sigma_p = \frac{K_c}{Z(a/c)\sqrt{\pi a}} \tag{15}$$

The predicted stress for each sample is plotted in Fig. 3 as a function of the measured fracture stress. A reasonable correlation is apparent.

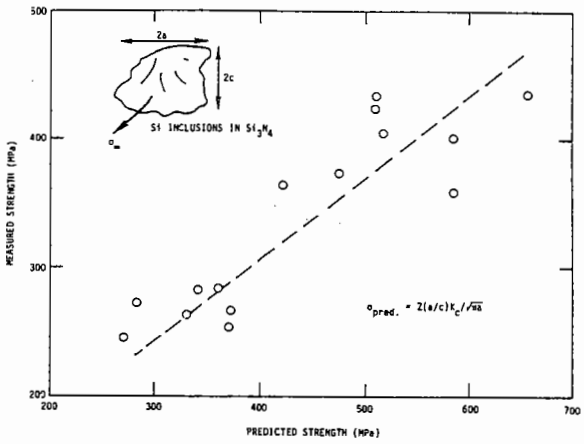

Fig. 3 A plot of the measured fracture strength of silicon inclusions as a function of the strength predicted by the subcritical cracking model.

A detailed statistical analysis has also been conducted to determine the level of correlation between the test data and the model. For this purpose, it has been supposed that the primary source of variability in the measured strength is the variation in fracture toughness of the matrix circumventing the inclusion (which could be very different from that of the remote matrix, because of an interaction zone). The inclusion/crack size is appreciably larger than the grain size. Hence, the variability in toughness is assumed to be normal. The fracture data are thus analyzed to determine their conformance to the normal distribution. (An alternative hypothesis attributes the strength variability to variations in the shape of the crack at the criticality; this possibility is not examined in the present analysis.)

The hypothetical model can be formally expressed as:

$$P_r[S<\zeta|\sigma_p = x] = \frac{1}{v\sqrt{2\pi}} \int_{-\infty}^{\zeta} \exp\left[-\frac{1}{2}\left(\frac{y-(\alpha+\beta x)}{v}\right)^2\right] dy \qquad (16)$$

where v^2 is the variance of the strength S for any given σ_p and P_r is the conditional distribution of strengths S; note that the conditional expectation of S, given σ_p, is assumed to be a linear function of σ_p,

$$(S|\sigma_p = x) = \alpha + \beta x + \varepsilon \qquad (17)$$

where ε is a random variable having mean zero and variance v^2. Applying the usual null hypothesis tests to the available data is complicated by the fact that the fracture data comprise 15 observations of 12 random variables. Specifically, only the residual

$$e = (S|\sigma_p = x) - \hat{\alpha} - \hat{\beta}x \qquad (18)$$

can be observed, where $\hat{\alpha}$ and $\hat{\beta}$ are the maximum likelihood estimates of α and β.

The normality of the fracture data are thus analyzed using two approaches: (a) by disregarding the variance-convariance structure of the residuals and (b) by obtaining independent residual observations using an orthogonal transformation of the fracture data.

The first method of analysis assumes that these residuals are independent. The variation in the magnitude of the residuals with the magnitude of the observation can then be obtained directly, as plotted in Fig. 4. There does not appear to be a systematic trend in the residuals (as verified by values of α_1 (skewness) = 0.04 and α_2 (excess) = -0.93), indicating that the normality hypothesis may be reasonable. Further, the residuals are arranged in increasing order of magnitude and plotted against the expected value of the i'th order statistic (Fig. 5). The good linearity of the plot tends to support the contention that the residuals are observations of a random variable having a normal distribution. Separate analysis of the data at large and small σ_p, using a procedure proposed by Goldfeld and Quandt[10], indicates that the residuals exhibit a systematic increase with increasing magnitude of the observation. This does not invalidate the normality of the distribution, but suggests a variance that increases as σ_p increases; a result that can be tentatively rationalized, as discussed below. However, it should be noted that the data may also conform with similar confidence to alternate models. The data analysis does not, therefore, provide a unique confirmation of the proposed fracture model.

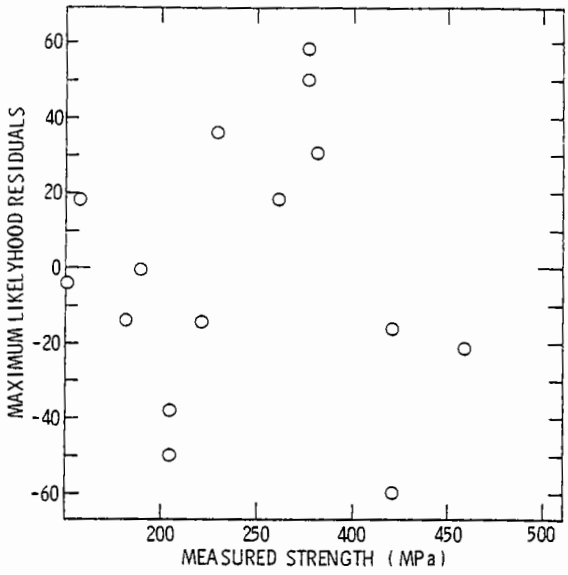

Fig. 4 A plot of the maximum likelihood residuals as a function of the measured strength.

The second method of analysis uses a procedure proposed by Henry Theil.[11] It involves an orthogonal transformation through an identity matrix. Only 13 residuals can be obtained because 2 degrees of freedom (slope and intercept) are sacrificed in the estimation procedure. The residuals obtained in this fashion exhibit precisely the same trends as the maximum likelihood residuals, as exemplified in Fig. 5.

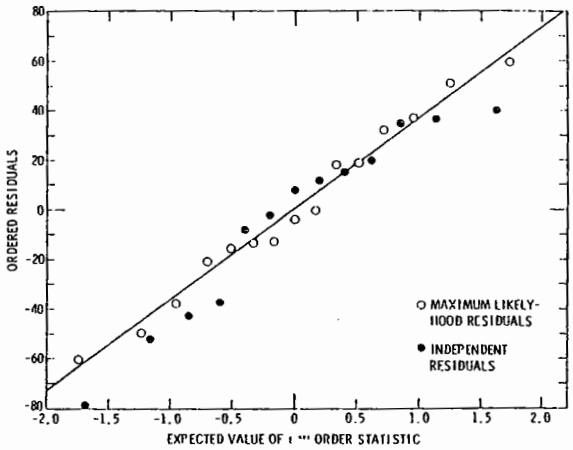

Fig. 5 A plot of the ordered residuals as a function of the estimate of the order statistic for both the maximum likelihood and the independent residuals.

It may be concluded, therefore, that the hypothesized fracture model, modified to allow for an increase in variance with increase in strength level, cannot be rejected by the data. However, this does not discount the possibility that the data might be also be consistent with an alternate fracture model. If the assumed fracture model is indeed valid, the parameters of the model implied by the data are: α = 99.655 MPa, β = 0.541. The deviation of β from unity suggests, within the context of the model, that the local toughness of the matrix may be lower than the remote macro-toughness of the matrix (i.e., ~ 3 MPa$\sqrt{m}$ instead of 5 MPa$\sqrt{m}$). This effect can be justified on the basis of a matrix locally degraded by interaction with the inclusion. The relative extent of the degradation may also be supposed to increase as the inclusion size decreases: accounting for the observed increase in variance with increase in strength level.

Iron Inclusion - Examination of the iron inclusions (Fig. 6) indicates that the inclusions contain several open cracks and/or porosity. The cracks and pores are presumably formed by diffusion within the inclusion (while at elevated temperatures) to relieve the stresses introduced by thermal expansion mismatch (Appendix I). An unrelieved thermal expansion mismatch strain ε_α will, of course, still develop at temperatures below those capable of sustaining rapid mass transport. The presence of the open cracks reduces the effective bulk modulus of the inclusion. The stresses within the inclusion, induced by the applied stress (Eq. 3) and the thermal expansion mismatch (Eq. 1), should thus be appreciably lower than would be anticipated from the intrinsic modulus of the iron silicide that comprises the inclusion. The low effective modulus also results in relatively large stresses in the matrix adjacent to the inclusion, comparable in form and magnitude to the stresses around a void. One possible failure model thus involves the activation of microcracks in the matrix, at the interface, by the enhanced tensile stress near the equatorial plane. The probability of fracture for this mode of failure can thus be expressed by the void fracture relation (Eq. 4), modified by a coefficient that depends upon the ratio of the inclusion modulus to the matrix modulus (c.f., Eq. 3).

Fig. 6 A scanning electron micrograph of a fractured iron inclusion in hot-pressed silicon nitride.

An alternate, or coupled, failure model supposes that a critical fracture condition is attained when the stress within the inclusion reaches the level required to extend one of the internal cracks: thereby excluding a subcritical inclusion fracture event. This hypothesis would be consistent with the lack of detectable acoustic emission prior to final fracture. The stress within the inclusion is a relatively uniform, hydrostatic tension p_i (or exactly uniform for an ellipsoidal inclusion) given by:

$$p_i = \psi\sigma_\infty + \sigma_\alpha \tag{19}$$

A weakest link model of inclusion fracture for a state of uniform tension would indicate a fracture probability,[12]

$$\Phi_i = 1 - \exp\left[-V_i \int_0^{p_i} g(S)dS\right] \tag{20}$$

where V_i is the volume of the inclusion ($=(4/3)\pi r^3$) and $g(S)dS$ is the distribution of flaw strengths that relates to the distribution of cracks within the inclusion (and the toughness of the inclusion). If we adopt the Weibull assumption, that $g(S)$ is given by:

$$\int_0^{p_i^c} g(S)dS = \left(\frac{p_i^c}{p_o}\right)^k \tag{21}$$

where p_o is a scale parameter and k a shape parameter, the inclusion fracture probability becomes:

$$\Phi_i = 1 - \exp\left[(4/3)\pi r^3 \left(\frac{\psi\sigma_\infty{}^c + \sigma_\alpha}{p_o}\right)^k\right] \tag{22}$$

where $\sigma_\infty{}^c$ is the applied stress at fracture.

Statistical analysis of the fracture results for iron inclusions, according to the procedure described above for void fracture, indicates that the maximum likelihood estimate of the radius coefficient, $\hat{\beta}$ is ~7. This value is larger than predicted by either of the above fracture models and thus excludes the existence of a single fracture model over the complete range of test results. A transition from one mechanism to another, as a function of defect size, may thus be occurring. The results can be rationalized by this hypothesis, but are too sparse to verify the existence of such a transition.

Tungsten Carbide Inclusions - The relatively minor effect of tungsten carbide inclusions on the fracture strength of silicon nitride precludes the need for a detailed statistical analysis of strength. The innocuous nature of these inclusions derives from a combination of relatively high toughness and modulus, as noted above. The analysis of fracture would involve considerations

of the distribution of microcracks located with the matrix in the small zone of tension near the poles of the inclusion.[8] The mode of analysis would be essentially similar to that conducted for fracture from voids[4,5], as modified by the different distribution of matrix stress and the presence of a high toughness inclusion.

IMPLICATIONS AND CONCLUSIONS

Good physical models of the probability of fracture from defects can greatly enhance the ability to predict failure from a nondestructive assessment of the defect type and size. Models pertinent to specific defect types have been presented, and correlations with fracture data have been attempted. The data are essentially consistent with the fracture models. However, to obtain good statistical confidence in the models, additional data are required, for well-controlled defect morphologies. Specifically, data sets are required for defects of a given size, taken at several different size values.

The present results can be used directly, within the probabilistic range encompassed by the data, even though the applicability of the models has not been substantiated (in each case) with good statistical confidence. The confident substantiation of the present (or alternative) models of fracture from defects would have the advantage of permitting the reliability predictions to be extended beyond the range of the data. Additionally, with self-consistent models and ample data, the variance would be minimized; thereby reducing the rejection probability for a given method of nondestructive analysis.[1]

The strong influence of the defect type on the fracture strength is re-emphasized. Specifically, tungsten carbide inclusions can be regarded as almost innocuous, while silicon inclusions are extremely deleterious (at least at low temperatures); iron inclusions and voids are of intermediate severity. It is interesting to note that surface cracks in hot-pressed silicon nitride produce about the same strength degradation as silicon inclusions with the same equivalent diameter. However, it should be noted that silicon develops appreciable toughness above ~1000°C, and melts at 1420°C. Silicon inclusions are thus likely to become less deleterious at elevated temperatures ($\gtrsim$ 900°C tending to approach the behavior of voids of equivalent size.

Finally, the appreciable dependence of the fracture probability on the inclusion type clearly emphasizes the importance of defect type classification for effective nondestructive failure prediction schemes.

APPENDIX I
STRESSES PRODUCED BY THERMAL EXPANSION MISMATCH

The magnitude of the thermal expansion mismatch stress depends on the cooling temperature ΔT (Eq. 1). An exact definition of this temperature differential presents several problems. The stress within the inclusion is purely hydrostatic (i.e., no shear stresses), and stress relaxation can only occur by mass transport processes. By contrast, the stress within the matrix has a zero hydrostatic component, $p(\sigma_{rr}+2\sigma_{\theta\theta}=0)$, but a very large shear component, $\sigma_{r\theta}(\equiv 3\beta^*/4)$; relaxation in the matrix can thus only occur by shear induced processes (e.g., grain boundary sliding accommodated by diffusive transport). The chemical potential that acts as the driving force for atom migration within the inclusion is dictated primarily by the hydrostatic pressure

$$\mu_i = -p\Omega \tag{A1}$$

where Ω is the atomic volume. The incidence of atom transport will modify the chemical potential and the stress distribution. This will occur primarily by vacancy transport to the interface. However, if the stress within the inclusion is tensile, cavities may nucleate by vacancy condensation.[13]

Once a cavity has nucleated, the stress at the cavity surface and the local chemical potential must be maintained at their equilibrium values

$$p = 2\gamma_s/r$$
$$\mu = -\Omega\gamma_s/r \tag{A2}$$

where r is the cavity radius. The chemical potential gradient now favors vacancy diffusion into the cavity, and cavity growth can be anticipated. Hence, if several cavities nucleate, the stresses within the inclusion remain at a moderate level, while mass transport is occurring. It should also be noted that the formation of cavities decreases the modulus of the inclusion. This tends to minimize the stresses which develop on cooling below the temperature at which mass transport eventually ceases.

APPENDIX II
A POSTERIORI MEASUREMENTS OF INCLUSION VOLUME

Most of the naturally occurring inclusions in structural ceramics develop cracks during temperature excursions. Consequently, the inclusions are relatively friable after fracture, and can be readily separated from the matrix by suitable etchants. The remaining void space can then be filled with a low density wax and the density of the ceramic/wax system measured in a density column. This density is directly related to the inclusion volume, v, the density of the ceramic host, ρ_c, and the density of the wax, ρ_w, as indicated below.

The measured density ρ' is:

$$\rho' = (M + m)/(V + v) \tag{A3}$$

where M is the mass of the ceramic, V its volume and m the mass of the wax contained within the void space. The parameters in Eq. (A3) that cannot be easily measured are m and V; these can be eliminated from the measurement process by substituting the densities ρ_w and ρ_c;

$$v = \left(\frac{M}{\rho_c}\right)\left[\frac{\rho_c - \rho'}{\rho' - \rho_w}\right] \qquad (A4)$$

The densities ρ_c and ρ' can be obtained directly from density column studies, before and after the wax has been inserted into the void space.

APPENDIX III
MAXIMUM LIKELIHOOD ESTIMATE OF SURVIVAL FUNCTION

Assume the survival function;

$$P[S \geq X|R=r] = \exp\left[-\int_0^X \lambda(u;r)du\right] \qquad (A5)$$

where

$$\lambda(u;r) = \lambda_0(u)g(r,\beta),$$

and $g(r,\beta)$ is of known form, except for β. Take

$$\lambda_0(u) = \sum_{k=1}^{\infty} a_k\, \delta(u-\xi_k), \qquad (A6)$$

where $0 < \xi_1 < \xi_2 \ldots\ldots$ is a net defined on R^+ (the positive real axis) that is dense enough to include all possible observations, and $\delta(.)$ is the Dirac δ function which is defined to be zero everywhere except at the point $\chi = 0$. In particular

$$\delta(x) = 0 \qquad \text{for} \quad x \neq 0$$

and

$$\int_{-\infty}^{\infty} \delta(x)\, dx = 1$$

It therefore follows that

$$P[S \geq x|R = r] = \exp\left[-\int_0^x \lambda_0(u)g(r,\beta)du\right]$$

$$= \exp\left[-g(r,\beta)\int_0^x \sum_{k=1}^{\infty} a_k\, \delta(u-\xi_k)du\right]$$

$$= \exp\left[-g(r,\beta) \sum_{\{k|\xi<X\}} a_k\right] \qquad (A7)$$

Hence the survival function is given as

$$P[S \geq x|R = r] = \prod_{\{k|\xi_k<x\}} \exp[-a_k g(r,\beta)] \qquad (A8)$$

Now, let F_i be the set of all test samples failing at epoch ξ_i, and R_i be the set of all test samples surviving up to $(\xi_i - 0)$. Then

$$P[F_i|R_i] = \prod_{j\in F_i} (1-\exp[-a_i g(r_j,\beta)]$$

$$\prod_{j\in R_i\setminus F_i} \exp[-a_i g(r_j,\beta)] \qquad (A9)$$

where r_j is the radius of the void in the j^{th} test sample. The total likelihood is then

$$L = \prod_{i=1}^{\infty} \left\{ \prod_{j\in F_i} (1-\exp[-a_i g(r_j,\beta)] \prod_{j\in R_i\setminus F_i} \exp[-a_i g(r_j,\beta)] \right\} \qquad (A10)$$

If no failures occur at epoch $j = k$, then the contribution to the total likelihood is

$$\prod_{j\in R_k\setminus\phi} \exp[-a_k g(r_j,\beta)]$$

which is maximum whenever $a_k = 0$ (since g (.) is a positive function). Therefore, restricting attention to those epochs at which failures do occur,

$$L = \prod_{k=1}^{N} \left\{ \left(1-\exp[-a_k g(r_{(k)},\beta)]\right) \prod_{k<\ell<N} \exp[-a_k g(r_{(\ell)},\beta)] \right\}, \qquad (A11)$$

$$\frac{\partial \ell n\, L}{\partial a_k} = 0 \qquad \text{for } k = 1, 2, \ldots\ldots \text{ or } N,$$

and denoting the estimate of a_r by $\hat{a}_r$, we have

$$\exp[-\hat{a}_k g(r_{(k)},\beta)] = 1 - \frac{g(r_{(k)},\beta)}{\sum_{k\leq\ell\leq N} g(r_{(\ell)},\beta)} \qquad (A12)$$

From (A8),

$$\hat{P}[S \geq x | R = r] \qquad \text{(A13)}$$

$$= \prod_{\{k \leq x\}} \left[1 - \frac{g(r_{(k)},\beta)}{\sum_{k \leq \ell \leq N} g(r_{(\ell)},\beta)} \right]^{g(r,\beta)/g(r_{(k)},\beta)}$$

for arbitrary radius r. If, in particular,

$$g(r,\beta) = r^{B},$$

then,

$$P[S \geq x | R = r]$$

$$= \prod_{\{k \leq x\}} \left[1 - \frac{r_{(k)}{}^{\beta}}{\sum_{k \leq \ell \leq N} r_{(\ell)}^{\beta}} \right]^{(r/r_{(k)})^{\beta}} \qquad \text{(A14)}$$

ACKNOWLEDGMENT

This research was sponsored by the Center for Advanced NDE, operated by the Science Center, Rockwell International, for the Defense Advanced Research Projects and the Air Force Materials Laboratory under Contract F33615-74-5180 and by the Army Materials and Mechanics Research Center under Contract DAAG46-76-0022.

REFERENCES

1. J.R. Richardson and A.G. Evans, to be published.
2. A.G. Evans, J. Mater. Sci., 9 (1976) 1145.
3. F.F. Lange, Fracture Mechanics of Ceramics (Ed. R.C. Bradt, D.P.H. Hasselman, F.F. Lange) Plenum, NY (1978) Vol. 4, p. 799.
4. O. Vardar, I. Finnie, D.R. Biswas and R.M. Fulrath, Int'l. J. Frac., 13 (1977) 215.
5. A.G. Evans, D.R. Biswas and R.M. Fulrath, J. Amer. Ceram. Soc., 62 (1979) 101.
6. J.B. Wachtman, W. Capps and J. Mandel, J. Materials, 7 (1972) 188.
7. J. Selsing, J. Amer. Ceram. Soc., 44 (1961) 149.
8. J.D. Eshelby, Proc. Roy. Soc., 241A (1958) 376.
9. D.R. Cox, Proc. Roy Stat. Soc., 34B (1972) 187.
10. S.M. Goldfield and R.E. Quandt, J. Amer. Statistical Assoc., 60 (1965) 539.
11. H. Theil, J. Amer. Statistical Assoc., 60 (1965) 1067.
12. J.R. Matthews, F.A. McClintock and W.J. Shack, J. Amer. Ceram. Soc., 59 (1976) 304.
13. A.G. Evans, J.R. Rice and J.P. Hirth, J. Amer. Ceram. Soc., in press.